IACS-010759, a potent inhibitor of glycolysis-deficient hypoxic tumor cells, inhibits mitochondrial respiratory complex I through a unique mechanism

Received for publication, March 6, 2020, and in revised form, April 13, 2020 Published, Papers in Press, April 14, 2020, DOI 10.1074/jbc.RA120.013366

Atsuhito Tsuji, Takumi Akao, Takahiro Masuya, Masatoshi Murai, and Hideto Miyoshi[1]

From the Division of Applied Life Sciences, Graduate School of Agriculture, Kyoto University, Kyoto 606-8502, Japan

Edited by Ruma Banerjee

The small molecule IACS-010759 has been reported to potently inhibit the proliferation of glycolysis-deficient hypoxic tumor cells by interfering with the functions of mitochondrial NADH-ubiquinone oxidoreductase (complex I) without exhibiting cytotoxicity at tolerated doses in normal cells. Considering the significant cytotoxicity of conventional quinone-site inhibitors of complex I, such as piericidin and acetogenin families, we hypothesized that the mechanism of action of IACS-010759 on complex I differs from that of other known quinone-site inhibitors. To test this possibility, here we investigated IACS-010759's mechanism in bovine heart submitochondrial particles. We found that IACS-010759, like known quinone-site inhibitors, suppresses chemical modification by the tosyl reagent AL1 of Asp^{160} in the 49-kDa subunit, located deep in the interior of a previously proposed quinone-access channel. However, contrary to the other inhibitors, IACS-010759 direction-dependently inhibited forward and reverse electron transfer and did not suppress binding of the quinazoline-type inhibitor [^{125}I]AzQ to the N terminus of the 49-kDa subunit. Photoaffinity labeling experiments revealed that the photoreactive derivative [^{125}I]IACS-010759-PD1 binds to the middle of the membrane subunit ND1 and that inhibitors that bind to the 49-kDa or PSST subunit cannot suppress the binding. We conclude that IACS-010759's binding location in complex I differs from that of any other known inhibitor of the enzyme. Our findings, along with those from previous study, reveal that the mechanisms of action of complex I inhibitors with widely different chemical properties are more diverse than can be accounted for by the quinone-access channel model proposed by structural biology studies.

Hypoxia is a well-recognized hallmark of different types of growing solid tumors (1, 2). Adaption to hypoxia is critical for tumor survival and growth. Response of mammalian cells to hypoxia is mediated by a family of transcription factors known as hypoxia-inducible factors (HIFs),[2] which regulate a large number of hypoxia-induced genes (3–5). Because HIF-1 plays a key role in tumor development and progression (5–7), it has been considered to be a potential druggable target for cancer therapy. Accordingly, many efforts have been devoted to screen for low-molecular-weight chemicals that modulate HIF-1 with desirable pharmacological properties and toxicity (safety) profiles required for useful pharmaceutical agents (8–12).

Ellinghaus *et al.* (10) identified BAY 87-2243 (Fig. 1) via high-throughput screening of a chemical library consisting of ~830,000 compounds using a luciferase-driven HIF-1 reporter cell line under hypoxia. BAY 87-2243 inhibited hypoxia-induced HIF-1 target gene expression in human lung cancer cell lines at low nanomolar concentrations without affecting the gene expressions that are not regulated by HIF-1/hypoxia. Extensive studies on the mechanism of action of BAY 87-2243 revealed that it modulates the HIF pathway by inhibiting mitochondrial NADH-ubiquinone oxidoreductase (respiratory complex I) and thereby reducing HIF protein levels under hypoxia (10). Afterward, Schöckel *et al.* (11) demonstrated that the inhibition of complex I by BAY 87-2243 is associated with the enhanced production of reactive oxygen species (ROS), a decrease in total ATP production, activation of AMP-activated protein kinase, and reduced viability of melanoma cells. They also showed that BAY 87-2243 treatment significantly reduces tumor growth in various BRAF mutant melanoma xenografts and patient-derived melanoma mouse models.

Through structural modification of BAY 87-2243, Molina *et al.* (12) produced a new complex I inhibitor, IACS-010759 (Fig. 1). They reported that treatment with IACS-010759 significantly inhibits proliferation and induces apoptosis in brain tumor and acute myeloid leukemia cells, which are largely dependent on oxidative phosphorylation for maintaining ATP levels. Metabolomic analyses suggested that the IACS-010759-mediated effects result from a combination of energy depletion and reduced aspartate production that leads to impaired nucle-

This work was supported by Japan Society for the Promotion of Science (JSPS) KAKENHI Grants JP18H02147 and JP19K22278 (to H. M.) and JP18K05458 (to M. M.). The authors declare that they have no conflicts of interest with the contents of this article.

This article contains Figs. S1–S4 and Schemes S1 and S2.

[1] To whom correspondence should be addressed: Division of Applied Life Sciences, Graduate School of Agriculture, Kyoto University, Kyoto 606-8502, Japan. Tel.: 81-75-753-6119; E-mail: miyoshi@kais.kyoto-u.ac.jp.

[2] The abbreviations used are: HIF, hypoxia-inducible factor; 49 kDa-Asp^{160}, Asp^{160} in the 49-kDa subunit; AL1, acetogenin ligand 1; AQ, amino-quinazoline; Asp-N, endoprotease Asp-N; AzQ, azido-quinazoline; Bistris, bis(2-hydroxyethyl)iminotris(hydroxymethyl)methane; BN-PAGE, blue native PAGE; CBB, Coomassie Brilliant Blue; complex I, proton-translocating NADH-quinone oxidoreductase; LDT, ligand-directed tosyl; Lys-C, lysylendopeptidase; ROS, reactive oxygen species; S1QEL, suppressor of site I_Q electron leak; SMP, submitochondrial particle; TAMRA, 6-carboxy-*N*,*N*,*N*′,*N*′-tetramethylrhodamine; TMH, transmembrane helix; UQ, ubiquinone; ANOVA, analysis of variance.

otide biosynthesis (12). In mouse models of brain cancer and acute myeloid leukemia, tumor growth was inhibited by IACS-010759 treatment at well-tolerated doses. However, a decrease in the core body temperature and death were observed at the highest doses in preclinical animal tests, which are anticipated effects of the excessive inhibition of oxidative phosphorylation (12). Molina *et al.* (12) also proposed that the binding position of IACS-010759 in complex I is the membrane-embedded ND1 subunit because amino acid substitution at Leu^{55} (to Phe) in this subunit, which faces the proposed ubiquinone-access channel interior (13) (see Fig. S1), took place in H292 clones with reduced susceptibility to IACS-010759 (reduced by 3–70-fold compared with parental cells). It is, however, still unclear whether IACS-010759 directly interacts with Leu^{55} if this mutation induces long-range structural changes in distant regions around the interface between the hydrophilic and membrane domains.

Thus, specific inhibitors of mitochondrial complex I are anticipated to become the seeds of anticancer agents for hypoxic tumors at well-tolerated doses. Regarding the energy metabolic background, hypoxic tumor cells with a reduced capacity for compensatory glycolysis may be more susceptible to the inhibition of oxidative phosphorylation (11, 12). If so, this view raises an important practical question: Do all complex I inhibitors have the potential to be anticancer agents? (Note that rotenone should be ruled out from this argument because this inhibitor is considered to elicit cytotoxicity not only by the inhibition of complex I but also by other mechanisms such as microtubule destabilization mediated by glycogen synthase kinase-3β (14). An answer to the question is not so simple because the balance between glycolysis and oxidative phosphorylation for ATP production is intricately regulated by multiple mechanisms that fluctuate via sensing concentrations of glucose, O_2, and ROS in tumor cells (15–17) and because cytotoxicity profiles required for practical pharmaceutical agents must be deliberated (11, 12). Taking the example of the latter, acetogenin and piericidin families, very strong natural inhibitors of mammalian complex I (18), exhibit potent antitumor activity to some tumor cell lines *in vitro*, whereas they also display significant cytotoxicity in normal cells (19–24). Nevertheless, in light of the tolerability of IACS-010759 in preclinical toxicity tests (12), we cannot rule out the possibility that a mechanism of the inhibitory action of IACS-010759 in complex I somewhat differs from that of other known quinone-site inhibitors and, consequently, this difference may be responsible for its relatively reduced cytotoxicity in normal cells. To advance biorational molecular design for new complex I inhibitors as promising seeds for anticancer drugs, it is essential to clarify the difference, if any, in the inhibitory action between IACS-010759 and known quinone-site inhibitors.

Therefore, here we investigated the action mechanism of IACS-010759 in bovine heart submitochondrial particles (SMPs) using three specific ligands as helpful benchmarks: AL1 (25, 26), [^{125}I]AzQ (27, 28), and [^{125}I]S1QEL1.1-PD1 (29), shown in Fig. S2, the binding positions of which have been defined in complex I. To identify the binding position of IACS-010759 in complex I, we also carried out photoaffinity labeling experiments using a photoreactive IACS-010759 derivative, [^{125}I]IACS-010759-PD1 (Fig. 1). The results obtained in this study revealed that the binding position of IACS-010759 in complex I is different from that of any other quinone-site inhibitors. IACS-010759 may not occupy the proposed binding cavity for quinone; rather, it may indirectly affect the quinone redox reactions by inducing structural changes of the quinone-binding pocket through binding to the middle of the ND1 subunit. This unique inhibitory action would be responsible for the interesting profiles of antitumor/cytotoxic activities of IACS-010759. Note that according to common terminology used in the complex I research field, we refer to the inhibitors that interfere with the terminal electron transfer step in complex I as "quinone-site inhibitors" throughout this work, although it is debatable whether all quinone-site inhibitors indeed occupy the proposed quinone-binding cavity (29, 30).

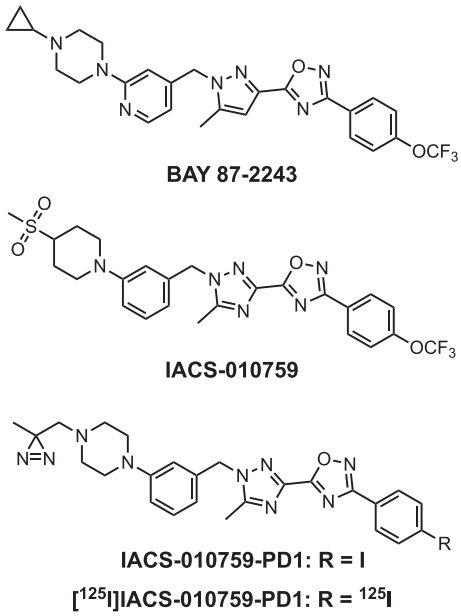

Figure 1. Structures of BAY 87-2243, IACS-010759, and [^{125}I]IACS-010759-PD1.

Results

Syntheses of IACS-010759 and its photoreactive analogue

IACS-010759 was synthesized in our laboratory by the method described in Scheme S1. To conduct photoaffinity labeling experiments, we also synthesized its photoreactive derivative [^{125}I]IACS-010759-PD1 (Fig. 1 and Scheme S2). [^{125}I]IACS-010759-PD1 possesses a diazirine ring and radioactive ^{125}I as a photolabile group and detecting tag, respectively. Introduction of ^{125}I makes it possible to conduct the labeling experiments with the lowest possible concentrations, thus minimizing the probability of nonspecific labeling that is a primary cause of false-positive results. Replacement of -OCF_3 (in IACS-010759) by -^{125}I (in [^{125}I]IACS-010759-PD1) may maintain hydrophobic nature of the right benzene ring moiety.

Inhibition of electron transfer in complex I by IACS-010759

We examined the inhibitory effect of IACS-010759 on the forward and reverse electron transfer in complex I using bovine heart SMPs. The forward electron transfer was evaluated as the

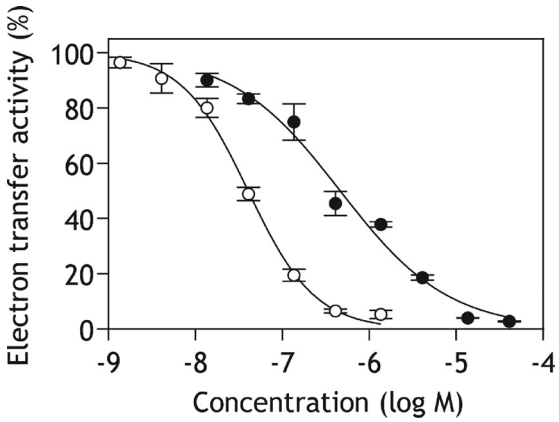

Figure 2. Dose-response curves for the inhibition of electron transfer in complex I by IACS-010759. The inhibition of forward (*closed circles*) and reverse (*open circles*) electron transfer by IACS-010759 was examined. The forward electron transfer reaction (NADH oxidase activity (0.60 ± 0.05 μmol of NADH/min/mg of proteins)) was initiated by adding NADH (final concentration: 50 μM) after the incubation of SMPs with IACS-010759 for 4 min at 30 °C. The reverse electron transfer reaction (ubiquinol-NAD^+ oxidoreduction (0.056 ± 0.004 μmol of NAD^+/min/mg of proteins)) was initiated by adding ATP (1.0 mM) after the incubation of SMPs with IACS-010759 for 4 min at 30 °C. The mitochondrial protein concentration was set at 100 μg/ml for both assays. Values in graphs are means ± S.E. (*error bars*) ($n = 3$).

NADH oxidase activity. The reverse electron transfer was assessed as the ubiquinol-NAD^+ oxidoreductase activity, which was driven by succinate oxidation with support of the proton motive force due to ATP hydrolysis. SMPs were incubated with IACS-010759 for 4 min before initiating the forward and reverse reactions by adding NADH (final concentration, 50 μM) and ATP (1.0 mM), respectively. As the reverse electron transfer is considerably slower than the forward electron transfer, the concentration of SMP proteins was set at a high level (100 μg/ml) for both assays.

The inhibitory potencies of IACS-010759 for the forward and reverse reactions, in terms of the IC_{50} value that is the molar concentration required to reduce the control activity by 50%, were 460 ± 45 and 41 ± 6 nM, respectively (Fig. 2), indicating that the inhibition of reverse electron transfer is more efficient (~10-fold) than that of the forward reaction. Thus, IACS-010759 turned out to elicit significant direction-dependent inhibition of electron transfer. Such significant direction dependence has not been reported for known quinone-site inhibitors. For example, the IC_{50} values of bullatacin (an acetogenin family member) for the forward and reverse electron transfer were 5.8 ± 0.4 and 4.6 ± 0.5 nM, respectively, under the same experimental conditions. Based on the quinone-access channel model in mammalian complex I (13), this result leads to a question of how IACS-010759 selectively interferes with one of the two opposite quinone-redox reactions that take place inside a common narrow cavity. On the other hand, IACS-010759 achieved almost complete inhibition (>95%) of both activities at high concentrations (Fig. 2), as observed for known potent quinone-site inhibitors.

Effects of IACS-010759 on the alkynylation of Asp^{160} in the 49-kDa subunit (49 kDa-Asp^{160}) by AL1

Ligand-directed tosyl (LDT) chemistry is a powerful method to covalently attach a chemical tag of choice to a target protein with high position specificity (31, 32). We previously demonstrated that 49 kDa-Asp^{160}, which is located deep inside the proposed quinone-access channel (13, 33, 34), can be specifically alkynylated (Asp^{160}(COO)-$(CH_2)_2$-C≡CH) through this technique using acetogenin-type ligand AL1 (Figs. S2 and S3) (25, 26). The pinpoint alkynylation can be achieved by incubating SMPs with AL1 for several hours and visualized by conjugating the fluorescent tag TAMRA-N_3 to Asp^{160}(COO)-$(CH_2)_2$-C≡CH via click chemistry after solubilizing SMPs (Fig. S3). The alkynylation was completely blocked by various quinone-site inhibitors (piericidin A, aminoquinazoline (AQ), bullatacin, and fenpyroximate) (25, 26).

To obtain an insight into the binding position of IACS-010759 in complex I, we examined the effects of IACS-010759 on the alkynylation of 49 kDa-Asp^{160} by AL1. SMPs were incubated with AL1 (0.10 μM) for 12 h at 35 °C in the presence of different concentrations of IACS-010759. IACS-010759 suppressed the alkynylation in a concentration-dependent manner (Fig. 3). BAY 87-2243 (30 μM), a parent compound of IACS-010759, also remarkably suppressed the chemical modification. As a reference, we confirmed that excess bullatacin (10 μM) that binds to the ND1 subunit completely blocks the alkynylation (Fig. 3).

Effects of IACS-010759 on the binding of [^{125}I]AzQ to the 49-kDa subunit

We previously showed that the quinazoline-type inhibitor [^{125}I]AzQ (Fig. S2) binds at the interface of the 49-kDa and ND1 subunits in bovine complex I (27, 28). The labeled regions in 49-kDa and ND1 were the N-terminal domain (Asp^{41}–Arg^{63}) and the matrix-side third loop connecting the transmembrane helices (TMHs) 5 and 6 (Asp^{199}–Lys^{262}), respectively, although radioactivity was predominantly distributed into the former. The binding of [^{125}I]AzQ to the enzyme was completely suppressed by other quinone-site inhibitors (rotenone, piericidin A, fenpyroximate, and bullatacin) (27).

We examined whether IACS-010759 suppresses the binding of [^{125}I]AzQ (5.0 nM) to the predominant target, the 49-kDa subunit. Notably, IACS-010759 did not suppress the binding of [^{125}I]AzQ up to 20 μM (4000-fold excess over [^{125}I]AzQ) (Fig. 4). Excess BAY 87-2243 (20 μM) also exhibited no influence on the labeling. We confirmed, as a reference, that AQ and bullatacin (5.0 μM each, 1000-fold) almost completely suppressed the binding of [^{125}I]AzQ (Fig. 4). These results strongly suggest that the binding position of IACS-010759 differs from that of traditional quinone-site inhibitors.

Effects of IACS-010759 on the binding of [^{125}I]S1QEL1.1-PD1 to the ND1 subunit

S1QELs (suppressors of site I_Q electron leak) are chemical suppressors of ROS production from the ubiquinone reaction site during reverse electron transfer through complex I in rat skeletal muscle mitochondria (35). S1QELs show no significant concomitant interferences with bioenergetic functions of mitochondria (including forward electron transfer) at their effective concentrations (35). Among S1QELs reported, S1QEL1.1 (Fig. S2) exhibited the suppressive effect at the lowest concentration range (~0.01 μM). To localize the binding position of S1QELs

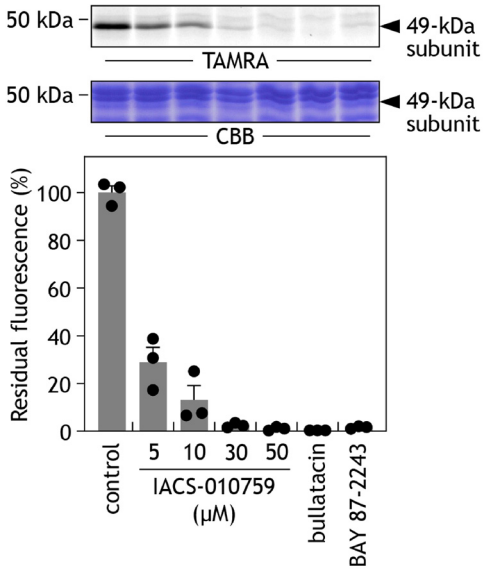

Figure 3. Effects of IACS-010759 on alkynylation of 49 kDa-Asp^{160} by AL1. Alkynylation of 49 kDa-Asp^{160} in SMPs (2.0 mg of proteins/ml) was performed via LDT chemistry using AL1 (0.10 μM) in the presence of different concentrations of IACS-010759. The alkynylation can be visualized by conjugating a fluorescent tag, TAMRA-N_3, to Asp^{160}(COO)-$(CH_2)_2$-C≡CH via click chemistry after solubilizing SMPs. Bullatacin (10 μM) and BAY 87-2243 (30 μM) were used as references. Approximately 30 μg of proteins were loaded in each well. *Top*, gel image of SDS-PAGE analysis used for LDT chemistry; *bottom*, the extent of suppression by test compounds. Values in graphs are means ± S.E. (*error bars*) (n = 3).

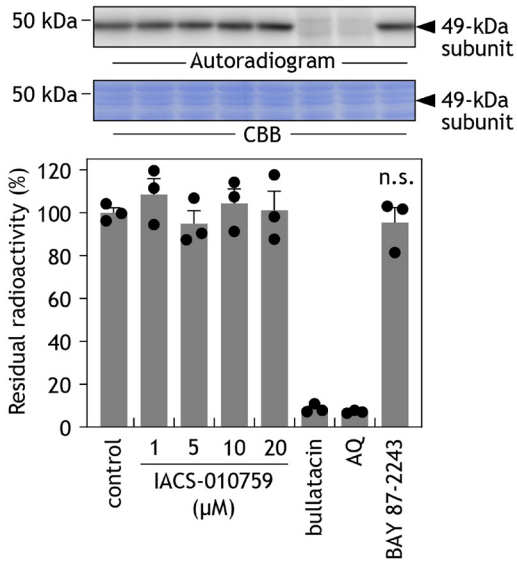

Figure 4. Effects of IACS-010759 on the specific binding of [^{125}I]AzQ to the 49-kDa subunit. The photoaffinity labeling of the 49-kDa subunit by [^{125}I]AzQ (5.0 nM) was carried out in SMPs (2.0 mg of proteins/ml) in the presence of different concentrations of IACS-010759 (up to 20 μM, 4000-fold excess). Bullatacin (5.0 μM), aminoquinazoline (5.0 μM), and BAY 87-2243 (20 μM) were used as references. Approximately 30 μg of proteins were loaded in each well. *Top*, gel image of SDS-PAGE analysis used for the photoaffinity labeling; *bottom*, the extent of suppression by test compounds. Values in graphs are means ± S.E. (*error bars*) (n = 3). *n.s.*, not significant compared with control (one-way ANOVA followed by Dunnett's test).

in bovine heart complex I, we previously conducted photoaffinity labeling experiments using a synthetic photoreactive derivative of S1QEL1.1 ([^{125}I]S1QEL1.1-PD1 (IC_{50} = 23 nM); Fig. S2) and found that [^{125}I]S1QEL1.1-PD1 binds to a region in the ND1 subunit, which is under the matrix-side third loop connecting TMHs 5–6 (29). We also showed that in contrast to known quinone-site inhibitors, S1QELs do not occupy the binding cavity for ubiquinone; rather, they may indirectly modulate the ubiquinone redox reactions through inducing structural changes of the cavity by binding to the middle of ND1 (29). Thus, [^{125}I]S1QEL1.1-PD1 is also a helpful benchmark sample for investigating the binding position of IACS-010759 in complex I.

We examined the effects of IACS-010759 on the specific binding of [^{125}I]S1QEL1.1-PD1 (5.0 nM) to the ND1 subunit. IACS-010759 suppressed the binding in a concentration-dependent manner (Fig. 5). However, the suppression was saturated at an incomplete level (~50%), and complete suppression was not achieved even in the presence of excess IACS-010759 (20 μM, 4000-fold). Similarly, ~20% radioactivity remained in the presence of excess BAY 87-2243 (20 μM). We previously demonstrated that fenpyroximate and AQ, which predominantly bind to the 49-kDa subunit (27, 28, 36), do not suppress the labeling by [^{125}I]S1QEL1.1-PD1, but bullatacin that binds to the ND1 subunit (37) almost completely suppresses the labeling (29). As a reference, the suppression by bullatacin (5.0 μM) is presented in Fig. 5. Overall, these results strongly suggest that IACS-010759 binds to the ND1 subunit, as proposed by Molina *et al.* (12), whereas the binding position of IACS-010759 in this subunit is not identical to that of S1QEL1.1, as further examined later.

The binding subunit of [^{125}I]IACS-010759-PD1 in complex I

To identify the binding subunit of IACS-010759 in bovine complex I, we conducted photoaffinity labeling experiments using photoreactive [^{125}I]IACS-010759-PD1 (Fig. 1), which was synthesized using IACS-010759 as a template. The IC_{50} value of [^{125}I]IACS-010759-PD1, determined in the NADH oxidase assay using its nonradioactive derivative, was 1700 ± 140 nM (with 100 μg of SMP proteins/ml). Although the inhibitory potency of [^{125}I]IACS-010759-PD1 decreased compared with IACS-010759 (460 nM), we offered this derivative to the photoaffinity labeling experiments because its IC_{50} value was at the one-digit micromolar level. Additionally, the IC_{50} value of [^{125}I]IACS-010759-PD1, determined in the reverse electron transfer reaction (with 100 μg of SMP proteins/ml), was 630 ± 34 nM, indicating that the direction dependence of the inhibitory potency of IACS-010759-PD1 (~3-fold) somewhat decreased compared with the parent IACS-010759 (~10-fold).

SMPs (4.0 mg of proteins/ml) were labeled by [^{125}I]IACS-010759-PD1 (10 nM) according to the method described under "Experimental procedures." The radiolabeled complex I was isolated by BN-PAGE, followed by resolution on doubled SDS gel using 10 and 16% Schägger-type SDS gels (38). The labeling by [^{125}I]IACS-010759-PD1 gave a major ~30-kDa radioactive spot above a diagonal axis (Fig. 6*A*), which corresponds to the position of the ND1 subunit (29). We verified this assignment by Western blotting using a rabbit anti-bovine ND1 antibody (Fig. 6*A*).

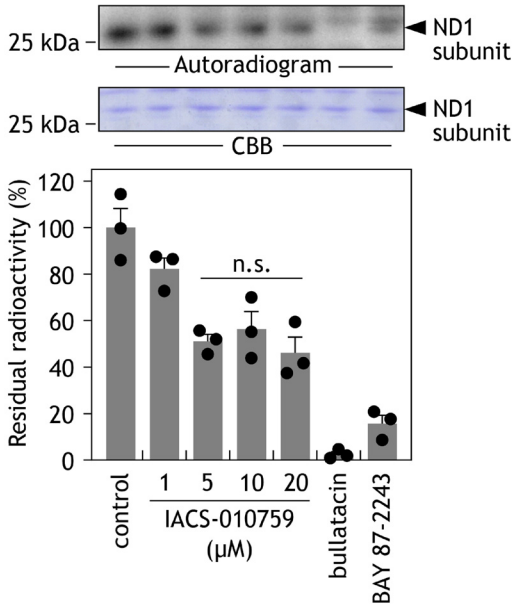

Figure 5. Effects of IACS-010759 on the specific binding of [^{125}I]S1QEL1.1-PD1 to the ND1 subunit. The photoaffinity labeling of the ND1 subunit by [^{125}I]S1QEL1.1-PD1 (5.0 nM) was carried out in SMPs (2.0 mg of proteins/ml) in the presence of different concentrations of IACS-010759 (up to 20 μM, 4000-fold excess), followed by the isolation of complex I by BN-PAGE and resolution of complex I subunits by SDS-PAGE. Bullatacin (5.0 μM) and BAY 87-2243 (20 μM) were used as references. Approximately 30 μg of proteins were loaded in each well. *Top*, gel image of SDS-PAGE analysis used for the photoaffinity labeling; *bottom*, the extent of suppression by test compounds. Values in graphs are means ± S.E. (*error bars*) (n = 3). *n.s.*, not significant among the three (one-way ANOVA followed by Tukey's test).

Effects of different ligands on the photoaffinity labeling by [^{125}I]IACS-010759-PD1

The effects of IACS-010759 on the specific binding of three benchmark ligands (AL1, [^{125}I]AzQ, and [^{125}I]S1QEL1.1-PD1) were examined in the above sections (Figs. 3–5). Here, we examined the effects of these ligands on the specific binding of [^{125}I]IACS-010759-PD1 (5.0 nM) to the ND1 subunit. An excess amount of IACS-010759 and BAY 87-2243 (5.0 μM each, 1000-fold molar excess) significantly suppressed the labeling by [^{125}I]IACS-010759-PD1 (Fig. 7). Approximately 30% of radioactivity in the control lane remained in the presence of excess S1QEL1.1 (5.0 μM), consistent with the result shown in Fig. 5. Excess bullatacin that binds to the ND1 subunit completely blocked the labeling, whereas fenpyroximate and AQ slightly (~20–30%) suppressed the labeling (Fig. 7). Considering high binding affinities of fenpyroximate and AQ to complex I (their IC_{50} values are one-digit nanomolar levels (27, 36)), it is reasonable to consider that their suppressive effects may be saturated at these low levels. Although IACS-010759 hardly suppressed the labeling by [^{125}I]AzQ (Fig. 4), AQ slightly suppressed the binding of [^{125}I]IACS-010759-PD1 (Fig. 7). This is probably because different pairs of inhibitors were examined in the two competition tests. Collectively, the results shown in Figs. 4 and 7 indicate that IACS-010759 and known inhibitors, which bind to the 49-kDa or PSST subunit, show only very limited interference with each other.

The binding position of [^{125}I]IACS-010759-PD1 in the ND1 subunit

To localize the position labeled by [^{125}I]IACS-010759-PD1 in the ND1 subunit, the labeled ND1 was isolated from the SDS gel and digested by lysylendopeptidase (Lys-C) or endoprotease Asp-N (Asp-N), whose theoretical cleavage sites (Lys and Asp) are few. The digestion by Lys-C and Asp-N gave major digests at ~16 and ~14 kDa, respectively (Fig. 6*B*). Based on the theoretical cleavage sites, the Lys-C and Asp-N digests may be the peptide Tyr^{127}–Lys^{262} (15.2 kDa) and Asp^{199}–Thr^{318} (13.8 kDa, containing an uncleavable site at Asp^{283} (29)), respectively (Fig. 6*C*). These results indicate that the position labeled by [^{125}I]IACS-010759-PD1 is assigned to the region Asp^{199}–Lys^{262} (Fig. 6*C*, *shadowed* in *yellow*), which includes the matrix-side third loop connecting TMHs 5 and 6, and TMHs 6 and 7 (Fig. 8*A*, *brown spheres*).

The quinazoline-type inhibitor [^{125}I]AzQ binds at the interface of the N terminus (Asp^{41}–Arg^{63}) of the 49-kDa subunit and the loop connecting TMHs 5 and 6 of the ND1 subunit (27, 28). The results shown in Figs. 4 and 7 indicate that IACS-010759 and quinazoline analogues do not affect each other's binding to complex I. Taking these facts into consideration, IACS-010759 (and [^{125}I]IACS-010759-PD1) may bind to a domain under this loop of ND1 (the loop Asp^{199}–Ala^{217} is shown in *red spheres* in the *right panels* in Fig. 8*A*). It is noteworthy that Leu^{55} in ND1, whose substitution (to Phe) reduced susceptibility to IACS-010759 (13), lies near the region labeled by [^{125}I]IACS-010759-PD1 (the labeled region is in *red* in Fig. 8*B*).

Although we were unable to pinpoint the residue(s) labeled by [^{125}I]IACS-010759-PD1 because of low reaction yields of a photoaffinity labeling technique, the labeled region (Asp^{199}–Lys^{262}) is identical to that labeled by [^{125}I]S1QEL1.1-PD2 (29). Nevertheless, the modes of inhibitory action are different between IACS-010759 and S1QELs, as discussed later.

Discussion

HIF-1 in hypoxic tumor cells is a potential druggable target for cancer therapy (5–7). Extensive efforts have been devoted to screen low-molecular-weight chemicals that modulate HIF-1 via inhibition of mitochondrial respiratory enzymes (8–12). Molina *et al.* (12) reported that IACS-010759 potently inhibits the proliferation of hypoxic tumor cells by interfering with the functions of respiratory complex I without exhibiting significant cytotoxicity in normal cells. Because mechanistic details of how IACS-010759 inhibits complex I remain to be elucidated, we herein addressed this issue via chemical biology approaches using bovine heart SMPs.

We found that IACS-010759, unlike traditional quinone-site inhibitors, exhibits the marked direction-dependent inhibition of electron transfer (the inhibition of reverse electron transfer was stronger than that of forward electron transfer; Fig. 2) and cannot suppress the binding of [^{125}I]AzQ to the N terminus of the 49-kDa subunit (Fig. 4). The photoaffinity labeling experiments revealed that IACS-010759 specifically binds to the region under the matrix-side third loop connecting TMHs 5–6 in the ND1 subunit (Figs. 6 and 8). These features resemble those elicited by S1QELs (29), which were originally reported to

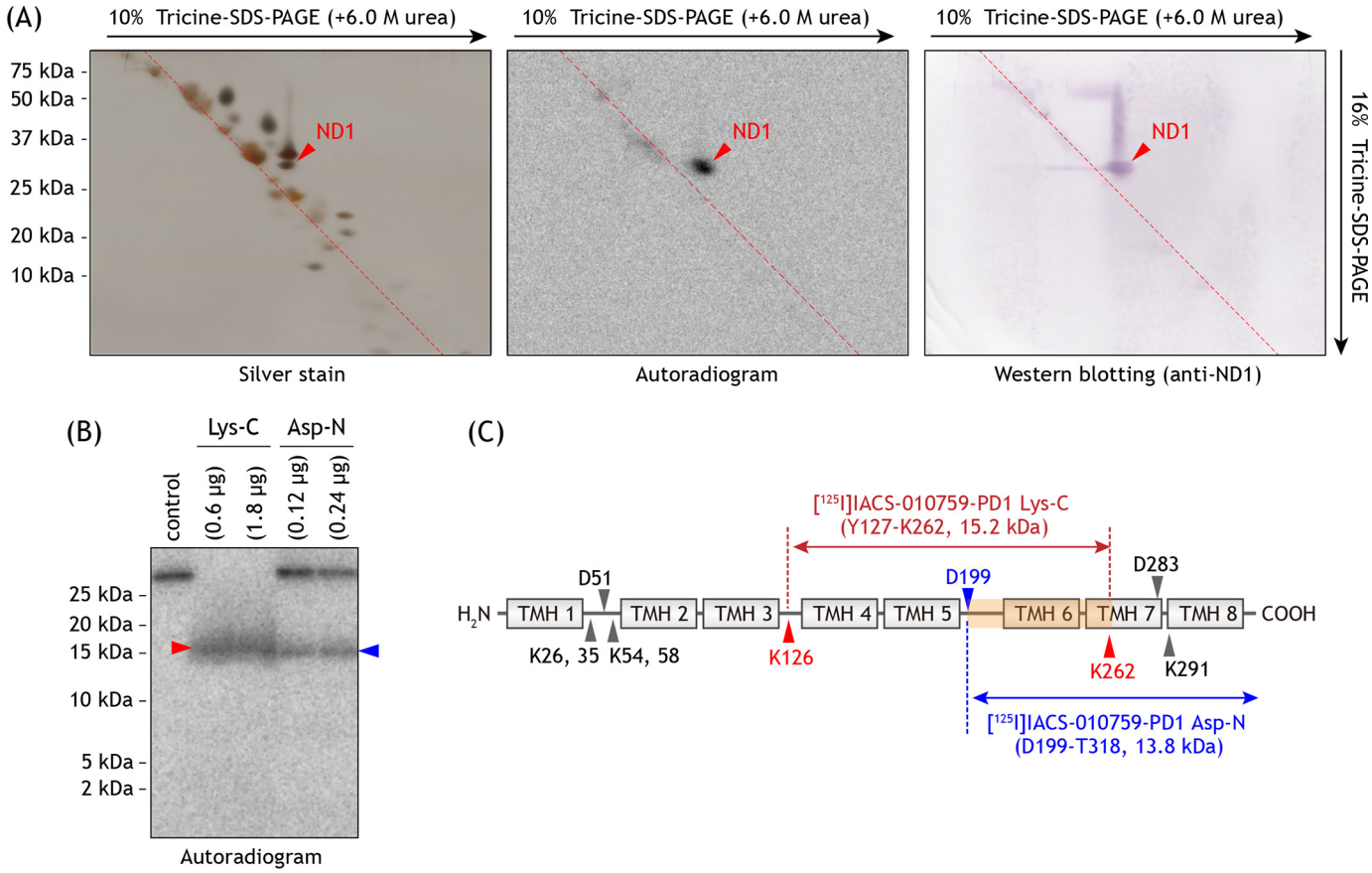

Figure 6. Photoaffinity labeling of complex I by [^{125}I]IACS-010759-PD1. *A*, SMPs (4.0 mg of proteins/ml) were cross-linked by [^{125}I]IACS-010759-PD1 (10 nM), followed by the purification of complex I by BN-PAGE and electroelution. Isolated complex I was resolved by doubled SDS-PAGE, and the SDS gel was subjected to silver staining, autoradiography, or Western blotting using anti-bovine ND1 antibody. All data are representative of three independent experiments. *B*, localization of the region labeled by [^{125}I]IACS-010759-PD1. The labeled ND1 subunit was digested by Lys-C or Asp-N. The digests were resolved on a 16% Schägger-type SDS gel (16% T, 6% C, containing 6.0 M urea), followed by autoradiography. Proteins equivalent to ~50 μg of SMPs were loaded into each well. All data are representative of three independent experiments. *C*, *schematic representation* of the digestion of ND1 by Lys-C or Asp-N. The TMHs were assigned according to the structures of bovine (13) or ovine (33) complex I. Predicted cleavage sites are denoted by *arrowheads* and marked with the residue numbers in the mature sequences of the bovine ND1 subunit (SwissProt entry P03887).

be specific suppressors of superoxide production from the quinone reaction site in complex I during reverse electron transfer (35). In fact, IACS-010759 and S1QEL derivatives competitively bound to the ND1 subunit despite the lack of definite structural similarity (Figs. 5 and 7), although complete suppression was not achieved even in the presence of an excess of either inhibitor. To explain the direction-dependent and incomplete (maximally ~30–80%) inhibition of electron transfer by S1QELs, we previously proposed that S1QELs do not occupy the binding cavity for ubiquinone; rather, they may *indirectly* affect the ubiquinone redox reactions by inducing structural changes of the cavity through binding to the middle of the ND1 subunit (29). Wong *et al.* (39) recently reported that the binding of S1QELs to complex I in rat skeletal muscle mitochondria (at concentrations exhibiting no electron transfer inhibition) influences conformation of the binding sites for rotenone and piericidin A, resulting in a decrease in the inhibitory potencies of both inhibitors. On the basis of comprehensive interpretations of the present results, it is likely that IACS-010759 also indirectly affects the ubiquinone redox reactions by binding to the ND1 subunit.

Nevertheless, it should be stressed that there are distinct differences in the inhibitory actions between IACS-010759 and S1QELs. First, IACS-010759, not S1QELs, suppressed the chemical modification of 49 kDa-Asp^{160} by AL1 (Fig. 3). Second, IACS-010759 attained complete inhibition (>95%) of both forward and reverse electron transfer (Fig. 2), whereas the extents of maximum inhibition by S1QELs, except S1QEL1.1, were saturated at incomplete levels (~30–80%) (29). Third, complete suppression was not achieved in the competition tests between [^{125}I]S1QEL1.1-PD1 and IACS-010759 (Fig. 5) or between [^{125}I]IACS-010759-PD1 and S1QEL1.1 (Fig. 7). The effects of IACS-010759 and S1QELs on the events that take place above the third loop connecting TMHs 5 and 6 in ND1 (*i.e.* quinone redox reactions (Fig. 2), the modification of 49 kDa-Asp^{160} by AL1 (Fig. 3), and the binding of [^{125}I]AzQ to the 49-kDa subunit (Fig. 4)) were summarized in Table 1, including bullatacin, which also binds to the ND1 subunit (37). It is evident that the effects of each of the three on the events were different from the other two. These findings strongly suggest that the structural changes in ND1 induced by the inhibitor binding dynamically propagate to the "upper" region (the PSST/49-kDa subunits) in different manners, depending on their binding positions reflecting varying chemical frameworks. A part of the third loop connecting TMHs 5 and 6 in ND1, which is in contact with the N terminus of the 49-kDa subunit,

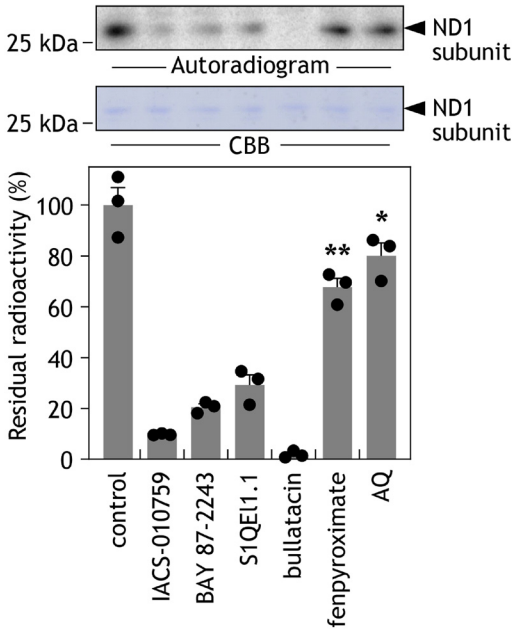

Figure 7. Effects of different inhibitors on the labeling of the ND1 subunit by [^{125}I]IACS-010759-PD1. The photoaffinity labeling of the ND1 subunit by [^{125}I]IACS-010759-PD1 (5.0 nM) was carried out in SMPs (2.0 mg of proteins/ml) in the presence of different inhibitors (5.0 μM each, 1000-fold), followed by the isolation of complex I by BN-PAGE and resolution of complex I subunits by SDS-PAGE. *Top*, gel image of SDS-PAGE analysis used for the photoaffinity labeling; *bottom*, the extent of suppression by test compounds. Values in graphs are means ± S.E. (*error bars*) ($n = 3$). *, $p < 0.05$; **, $p < 0.001$ compared with control (one-way ANOVA followed by Dunnett's test).

is disordered in X-ray crystallographic and cryo-EM structures (13, 33, 40, 41). This flexible loop could mediate the dynamic propagation. Taken together, we conclude that the manner of action of IACS-010759 is unique and different from that not only of traditional quinone-site inhibitors but also of S1QELs.

Molina *et al.* (12) proposed that IACS-010759 enters the proposed quinone-access channel because the L55F mutation in the ND1 subunit in H292 clones leads to moderate resistance to IACS-010759 (4–70-fold compared with parental cells). Based on the structural model of bovine complex I (13), this residue lies close to the entrance of the channel (Fig. S1). If IACS-010759 enters the channel and is in direct contact with Leu^{55}, the channel is almost completely covered by this compound. In that case, quinazoline-type inhibitors (such as [^{125}I]AzQ), which are supposed to enter and transit to near the "top" of the channel (40, 42), would no longer enter the channel, but this was not the case. An excess amount of IACS-010759 did not suppress the binding of [^{125}I]AzQ to the 49-kDa subunit (Fig. 4). This result also suggests that the manner of action of IACS-010759 cannot be explained simply by the scenario based on the channel model. Nonetheless, we do not exclude the possible contribution of Leu^{55} to the inhibitory action of IACS-010759 because this residue lies near the binding region of IACS-010759 identified in this study (Fig. 8*B*). We will further discuss the action mechanisms of a variety of complex I inhibitors with relevance to the quinone-access channel model below.

Mitochondrial complex I is a promising target not only for anticancer drugs (10–12) but also for anthelmintic reagents (43, 44) and agrochemicals (45, 46). Structural biology studies have proposed that quinone-site inhibitors enter into a narrow and long (~30 Å) quinone-access channel and prevent the catalytic reaction of quinone by being "caged" inside the channel (40, 47). This proposal was originally derived from electron density attributed to bound piericidin A, which was observed to overlie electron density attributed to bound *n*-decyl-ubiquinone in crystallographic maps from *Thermus thermophilus* complex I (48). It should be realized, however, that this view of the binding of quinones or inhibitors has yet to be established experimentally. We note that excess piericidin A (up to 4000-fold) partially suppressed the binding of [^{125}I]IACS-010759-PD1 to complex I (by ~60%) but hardly affected the binding of [^{125}I]S1QEL1.1-PD1 (Fig. S4). Through photoaffinity labeling experiments using different types of quinone-site inhibitors, we previously demonstrated that the inhibitors do not necessarily enter the proposed channel; rather, they bind *around* the channel (30). The present and previous (29) studies disclosed diverse binding positions of new inhibitors of complex I (*i.e.* IACS-010759 and S1QELs), which do not overlap with those of known quinone-site inhibitors. Taken together, the action mechanisms of complex I inhibitors with widely different chemical frameworks are far more diverse than hitherto considered based on the channel model (13, 40, 47, 48). We recently demonstrated that complex I in bovine SMPs can catalytically reduce oversized ubiquinones, which are highly unlikely to transit the narrow channel because their side chain includes a significantly bulky block (30, 49). This fact may call into question whether the current channel model fully reflects the physiologically relevant states. The cryo-EM structure of *Yarrowia lipolytica* complex I showed a tightly bound UQ_9 molecule in the proposed quinone-access tunnel (50). However, as the position of the head-ring of the bound UQ_9 is at distance from the Fe-S cluster N2 (~27 Å), the functional significance of the observed position of UQ_9 in the catalytic cycle remains to be elucidated.

The present study was initiated to answer the question of why IACS-010759, unlike other traditional quinone-site inhibitors, can elicit antitumor activity in glycolysis-deficient tumor cells by inhibiting complex I *without* displaying significant cytotoxicity in normal cells at tolerated doses (12). To answer this question, many critical factors in different cell lines must be considered, such as the balance between glycolysis and oxidative phosphorylation for ATP production and superoxide generation involved in the inhibition of electron transfer (both forward and reverse). Regarding superoxide generation, inhibitors of the ubiquinone reaction step in complex I elicit opposite effects, depending on the direction of electron transfer; namely, they enhance and reduce superoxide generation during the forward and reverse electron transfer, respectively (51, 52). Moreover, although IACS-010759 inhibits the reverse electron transfer more efficiently (by ~10-fold) than the forward electron transfer (Fig. 2), it is unclear whether, and how much, the reverse electron transfer occurs in intact cells under conditions that favor forward electron flux through

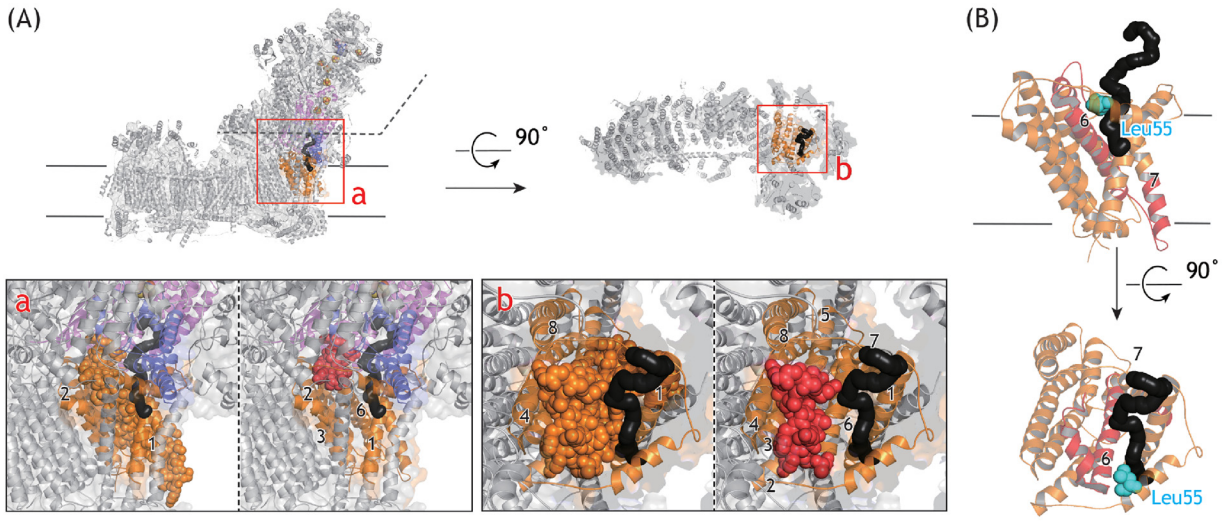

Figure 8. The region labeled by [^{125}I]IACS-010759-PD1 in the ND1 subunit. *A*, [^{125}I]IACS-010759-PD1 labeled the region Asp^{199}–Lys^{262} (*brown spheres*) in the ND1 subunit (*brown*). The third loop connecting the TMHs 5 and 6 (Asp^{199}–Ala^{217}) is presented in *red spheres* on the *right*. The 49-kDa and PSST subunits are shown in *pink* and *purple*, respectively. Here, we used the structural model of ovine complex I (Protein Data Bank entry 5LNK) (33) because the third loop of ND1 is disordered in the deactive state of the bovine enzyme (13). The quinone-access channel proposed in the current models was generated using MOLE with a 1.4-Å probe (RRID:SCR_018314) (61) and is shown in *black*. The hydrophilic domain *above* the *dotted line* shown in *a* was deleted in *b* for clarity. *B*, *close-up* of the ND1 subunit (*brown*). The positions of Leu^{55} (a *space-filling model* in *cyan*) and the region labeled by [^{125}I]IACS-010759-PD1 (Asp^{199}–Lys^{262} in *red*) are shown with the quinone-access channel (*black*).

Table 1
Effects of inhibitors on the events that take place above the third loop connecting TMHs 5 and 6 in the ND1 subunit

Inhibitors	Modification of 49 kDa-Asp^{160}[a]	Binding of [^{125}I]AzQ[b]	Inhibition of electron transfer[c]
IACS-010759	Suppress	Not suppress	Complete
S1QELs	Not suppress	Not suppress	Incomplete[d]
Bullatacin[e]	Suppress	Suppress	Complete

[a] Effects of the inhibitors on the chemical modification of 49 kDa-Asp^{160} by AL1.
[b] Effects of the inhibitors on the specific binding of [^{125}I]AzQ to the N terminus of the 49-kDa subunit.
[c] The extent of inhibition of the forward and reverse electron transfer. IACS-010759 and bullatacin almost completely inhibit both activities (>95%).
[d] The extents of maximum inhibition by S1QELs were saturated at incomplete levels (~30–80%), except S1QEL1.1 (29).
[e] Conventional quinone-site inhibitors (aminoquinazoline, fenpyroximate, piericidin A, and rotenone) exhibit the same effects as those of bullatacin (25, 29, 30).

complex I (12, 51, 52). (Note that there is indirect evidence that the reverse electron transfer is an important physiological process that underlies mitochondrial redox signaling under various conditions (53, 54).) With all things combined, it may be practically impossible to precisely predict how IACS-010759 treatment affects the total ATP production and superoxide generation at the cell level. Therefore, we currently have no definite answer to the question above. Nevertheless, the present study revealed IACS-010759 to be a unique inhibitor of complex I, the manner of action of which is different from that of any other quinone-site inhibitors. This unique manner of action of IACS-010759 at the enzyme level may be responsible for its interesting profiles of antitumor/cytotoxic activities. Besides IACS-010759 and BAY 87-2243, recent cancer chemotherapeutic studies showed that a cellular target of mubritinib (an inhibitor of acute myeloid leukemia (55); Fig. S1) and quinazoline diones (inhibitors of non-small-cell lung carcinoma (56); Fig. S1) is also mitochondrial complex I. Given the diverse manners of action of complex I inhibitors, there could be considerable room for producing further unique inhibitors (or modulators) that elicit a broad spectrum of biological activities.

Experimental procedures

Materials

Bullatacin, piericidin A, and fenpyroximate were kindly provided by J. L. McLaughlin (Purdue University, West Lafayette, IN), S. Yoshida (RIKEN, Saitama, Japan), and Nihon Nohyaku Co., Ltd. (Tokyo, Japan), respectively. Acetogenin-type ligand (AL1) was the same sample as that used previously (32). [^{125}I]AzQ was synthesized by the previously reported procedure (27, 28). BAY 87-2243 was purchased from ChemScene (Monmouth Junction, NJ). Protein standards (Precision Plus Protein Standards) for SDS-PAGE were purchased from Bio-Rad. [^{125}I]NaI was purchased from PerkinElmer Life Sciences. All other reagents were analytical grade.

Preparation of bovine heart SMPs and measurement of complex I activity

Mitochondria were isolated from bovine heart. SMPs were prepared by the method of Matsuno-Yagi and Hatefi (57) and stored in buffer containing 250 mM sucrose and 10 mM Tris-HCl (pH 7.4) at −80 °C until used. The NADH oxidase activity (forward electron transfer) in SMPs was measured spectrometrically with a Shimadzu UV-3000 instrument (340 nm, ϵ = 6.2 mM^{-1} cm^{-1}) at 30 °C (29). The reaction was initiated by adding 50 μM NADH after the equilibration of SMP with an inhibitor for 4 min. The reaction medium (2.5 ml) contained 0.25 M sucrose, 1.0 mM $MgCl_2$, and 50 mM phosphate buffer (pH 7.4). The final mitochondrial protein concentration was set to 30 or 100 μg of proteins/ml, depending on the experimental purpose. The IC_{50} values of inhibitors were calculated by Prism (version 8, GraphPad Software, La Jolla, CA) using sigmoid dose-response curve fitting.

Measurement of reverse electron transfer in complex I

The reverse electron transfer (ubiquinol-NAD^+ oxidoreductase activity) was driven by the oxidation of succinate and hydrolysis of ATP (58). The reaction was measured spectrophotometrically by following the reduction of NAD^+ with a Shimadzu UV-3000 spectrophotometer (340 nm, $\epsilon = 6.2\ mM^{-1}\ cm^{-1}$) at 30 °C. The reaction was initiated by the addition of 1.0 mM ATP after the equilibration of SMP with an inhibitor for 4 min. The reaction medium (2.5 ml) contained 0.25 M sucrose, 7.0 mM sodium succinate, 6.0 mM $MgCl_2$, 1.0 mM KCN, 1.0 mM NAD^+, and 50 mM Tris-HCl (pH 7.5), and the final protein concentration of SMPs was 100 μg/ml. We confirmed that the reverse electron transfer is fully sensitive to SF6847 (protonophoric uncoupler) or oligomycin (ATP synthase inhibitor).

Alkynylation of complex I in SMPs by AL-1 (ligand-directed tosyl chemistry)

Bovine SMPs (2.0 mg of protein/ml, 100–200 μl), suspended in a buffer containing 250 mM sucrose, 1.0 mM $MgCl_2$, and 50 mM KP_i (pH 7.4), were incubated with AL1 (0.10 μM) in the presence or absence of a competitor for 12 h at 35 °C (25). SMPs were then collected by ultracentrifugation (200,000 × *g*, 20 min, 4 °C) and denatured in 1.0% (w/v) SDS (25–50 μl). To visualize the proteins alkynylated by AL1, they were conjugated with a fluorescent TAMRA-N_3 tag via Cu^+-catalyzed click chemistry using the Click-iT reaction buffer kit (Life Technologies, Inc.) according to the manufacturer's protocols. Proteins were recovered by precipitation with methanol/chloroform (4:1, v/v) and subjected to Laemmli-type 12.5% SDS-PAGE, followed by Coomassie Brilliant Blue (CBB) stain and fluorescent gel imaging.

Photoaffinity labeling of complex I in SMPs by [^{125}I]AzQ, [^{125}I]S1QEL1.1-PD1, and [^{125}I]IACS-010759-PD1

Bovine SMPs (2.0 mg/ml, 100 μl), which were previously incubated with a competitor of choice at room temperature for 10 min, were incubated with [^{125}I]AzQ (5.0 nM) in buffer containing 250 mM sucrose, 50 mM KP_i (pH 7.4), and 5.0 mM $MgCl_2$ at room temperature for 10 min, and then 50 μM NADH was added for a further 5 min. The mixture was then irradiated with a long wavelength UV-lamp (Black-lay model B-100A, UVP, Upland, CA) on ice for 10 min at a distance of 10 cm from the light source (27). The reaction was quenched by the addition of 4× Laemmli sample buffer (34 μl). Samples were separated on a 12.5% Laemmli gel, which was stained with CBB, dried, exposed to an imaging plate (BAS-MS2040, Fujifilm, Tokyo, Japan), and visualized with the Bio-imaging analyzer FLA-5100 (Fujifilm) or Typhoon-FLA 9500 (GE Healthcare, Buckinghamshire, UK). The incorporated radioactivity of each band was quantified using Multi Gauge (Fujifilm) or ImageQuant (GE Healthcare). The photoaffinity labeling experiments by [^{125}I]S1QEL1.1-PD1 and [^{125}I]IACS-010759-PD1 in the presence or absence of a competitor were conducted by the same procedures as those for [^{125}I]AzQ above, with the exception that the labeled complex I was isolated by BN-PAGE and it was further separated on a SDS gel.

Identification of the subunit labeled by [^{125}I]IACS-010759-PD1

SMPs labeled by [^{125}I]IACS-010759-PD1 (10 nM) were solubilized in sample buffer containing 50 mM Bistris-HCl (pH 7.2), 50 mM NaCl, 10% (w/v) glycerol, 1.0% (w/v) dodecyl maltoside, and 0.001% (w/v) Ponceau S on ice for 1 h, and the samples were separated by BN-PAGE (30) using a 4–16% precast gel system (Life Technologies) according to the manufacturer's protocol. The isolated complex I was further solved on a Laemmli-type 12.5% SDS gel (59) or Schägger-type 10% SDS gel containing 6.0 M urea (60).

Doubled SDS-PAGE was conducted as described previously (30, 38). In brief, the labeled complex I was separated on a first-dimensional 10% Schägger-type gel (10% T, 3% C, containing 6.0 M urea). The gel slice was then acidified with 100 mM Tris-HCl (pH 2.0) for 30 min, followed by second-dimensional separation on a 16% Schägger-type gel (16% T, 3% C). Typically, complex I equivalent to 200 μg of SMPs was separated on a mini-size gel (80 × 90 mm, 1 mm). The resolved proteins were visualized by MS-compatible silver staining (Wako Silver stain MS kit, Wako Pure Chemicals, Osaka), followed by autoradiography.

To detect the ND1 subunit, proteins were separated on a Schägger-type SDS gel and transferred onto a polyvinylidene difluoride membrane (27, 60). The membrane was blocked with 1% (w/v) gelatin in TBS buffer (10 mM Tris-HCl buffer (pH 7.4) and 0.9% (w/v) NaCl) containing 0.5% (w/v) Tween 20 (Tween TBS) and then probed with a rabbit anti-bovine ND1 antibody (a kind gift from Dr. Takao Yagi, Scripps Research Institute, La Jolla, CA), followed by incubation with the alkaline phosphatase–conjugated anti-rabbit secondary antibody (Sigma–Aldrich). The membrane was washed three times with Tween TBS and developed with nitro blue tetrazolium/5-bromo-4-chloro-3-indolyl phosphate colorimetric reagents (Bio-Rad). The primary and secondary antibodies were diluted with Tween TBS at the ratios of 1:3000 and 1:8000, respectively.

Proteomic analysis

For the exhaustive digestion of the ND1 subunit, the subunit labeled by [^{125}I]IACS-010759-PD1 was recovered from the gel by electroelution in 10 mM Tris-HCl buffer (pH 8.0) containing 0.025% (w/v) SDS. The partially purified ND1 subunit was digested with lysylendopeptidase (Wako Pure Chemicals, Osaka, Japan) or endoprotease Asp-N (Roche Applied Science) in 50 mM Tris-HCl buffer (pH 8.5) containing 0.1% SDS or 50 mM NaP_i buffer (pH 8.0) containing 0.01% SDS, respectively. The digests were resolved on a Schägger-type SDS gel (60), followed by autoradiography.

Data availability

All data are contained within the article and associated supporting information.

Author contributions—A. T., T. A., T. M., M. M., and H. M. data curation; A. T., T. A., T. M., M. M., and H. M. formal analysis; A. T., T. A., T. M., M. M., and H. M. investigation; A. T., M. M., and H. M. writing-original draft; M. M. and H. M. conceptualization; M. M. and H. M. supervision; M. M. and H. M. funding acquisition.

Acknowledgment—We acknowledge the Radioisotope Research Center, Kyoto University, for technical support in the radioisotope experiments.

References

1. Höckel, M., and Vaupel, P. (2001) Tumor hypoxia: definitions and current clinical, biologic, and molecular aspects. *J. Natl. Cancer Inst.* **93,** 266–276 CrossRef Medline
2. Cantor, J. R., and Sabatini, D. M. (2012) Cancer cell metabolism: one hallmark, many faces. *Cancer Discov.* **2,** 881–898 CrossRef Medline
3. Gordan, J. D., and Simon, M. C. (2007) Hypoxia-inducible factors: central regulators of the tumor phenotype. *Curr. Opin. Genet. Dev.* **17,** 71–77 CrossRef Medline
4. Semenza, G. L. (2010) HIF-1: upstream and downstream of cancer metabolism. *Curr. Opin. Genet. Dev.* **20,** 51–56 CrossRef Medline
5. Hu, J., Locasale, J. W., Bielas, J. H., O'Sullivan, J., Sheahan, K., Cantley, L. C., Vander Heiden, M. G., and Vitkup, D. (2013) Heterogeneity of tumor-induced gene expression changes in the human metabolic network. *Nat. Biotechnol.* **31,** 522–529 CrossRef Medline
6. Wenger, R. H. (2002) Cellular adaptation to hypoxia: O_2-sensing protein hydroxylases, hypoxia-inducible transcription factors, and O_2-regulated gene expression. *FASEB J.* **16,** 1151–1162 CrossRef Medline
7. Poellinger, L., and Johnson, R. S. (2004) HIF-1 and hypoxic response: the plot thickens. *Curr. Opin. Genet. Dev.* **14,** 81–85 CrossRef Medline
8. Lin, X., David, C. A., Donnelly, J. B., Michaelides, M., Chandel, N. S., Huang, X., Warrior, U., Weinberg, F., Tormos, K. V., Fesik, S. W., and Shen, Y. (2008) A chemical genomics screen highlights the essential role of mitochondria in HIF-1 regulation. *Proc. Natl. Acad. Sci. U.S.A.* **105,** 174–179 CrossRef Medline
9. Li, S. H., Shin, D. H., Chun, Y.-S., Lee, M. K., Kim, M.-S., and Park, J.-W. (2008) A novel mode of action of YC-1 in HIF inhibition: stimulation of FIH-dependent p300 dissociation from HIF-1a. *Mol. Cancer Ther.* **7,** 3729–3738 CrossRef Medline
10. Ellinghaus, P., Heisler, I., Unterschemmann, K., Haerter, M., Beck, H., Greschat, S., Ehrmann, A., Summer, H., Flamme, I., Oehme, F., Thierauch, K., Michels, M., Hess-Stumpp, H., and Ziegelbauer, K. (2013) BAY 87-2243, a highly potent and selective inhibitor of hypoxia-induced gene activation has antitumor activities by inhibition of mitochondrial complex I. *Cancer Med.* **2,** 611–624 CrossRef Medline
11. Schöckel, L., Glasauer, A., Basit, F., Bitschar, K., Truong, H., Erdmann, G., Algire, C., Hägebarth, A., Willems, P. H. G. M., Kopitz, C., Koopman, W. J. H., and Héroult, M. (2015) Targeting mitochondrial complex I using BAY 87-2243 reduced melanoma tumor growth. *Cancer Metab.* **3,** 11 CrossRef Medline
12. Molina, J. R., Sun, Y., Protopopova, M., Gera, S., Bandi, M., Bristow, C., McAfoos, T., Morlacchi, P., Ackroyd, J., Agip, A. A., Al-Atrash, G., Asara, J., Bardenhagen, J., Carrillo, C. C., Carroll, C., *et al.* (2018) An inhibitor of oxidative phosphorylation exploits cancer vulnerability. *Nat. Med.* **24,** 1036–1046 CrossRef Medline
13. Zhu, J., Vinothkumar, K. R., and Hirst, J. (2016) Structure of mammalian respiratory complex I. *Nature* **536,** 354–358 CrossRef Medline
14. Hongo, H., Kihara, T., Kume, T., Izumi, Y., Niidome, T., Sugimoto, H., and Akaike, A. (2012) Glycogen synthase kinase-3β activation mediates rotenone-induced cytotoxicity with the involvement of microtubule destabilization. *Biochem. Biophys. Res. Commun.* **426,** 94–99 CrossRef Medline
15. Koppenol, W. H., Bounds, P. L., and Dang, C. V. (2011) Otto Warburg's contributions to current concepts of cancer metabolism. *Nat. Rev. Cancer* **11,** 325–337 CrossRef Medline
16. Birsoy, K., Wang, T., Chen, W. W., Freinkman, E., Abu-Remaileh, M., and Sabatini, D. M. (2015) An essential role of the mitochondrial electron transport chain in cell proliferation is to enable aspartate synthesis. *Cell* **162,** 540–551 CrossRef Medline
17. Weinberg, S. E., and Chandel, N. S. (2015) Targeting mitochondria metabolism for cancer therapy. *Nat. Chem. Biol.* **11,** 9–15 CrossRef Medline
18. Miyoshi, H., Ohshima, M., Shimada, H., Akagi, T., Iwamura, H., and McLaughlin, J. L. (1998) Essential structural factors of annonaceous acetogenins as potent inhibitors of mitochondrial complex I. *Biochim. Biophys. Acta* **1365,** 443–452 CrossRef Medline
19. Bermejo, A., Figadere, B., Zafra-Polo, M.-C., Barrachina, I., Estornell, E., and Diego Cortes, D. (2005) Acetogenins from *Annonaceae*: recent progress in isolation, synthesis and mechanisms of action. *Nat. Prod. Rep.* **22,** 269–303 CrossRef Medline
20. Kojima, N., Hayashi, H., Suzuki, S., Tominaga, H., Maezaki, N., Tanaka, T., and Yamori, T. (2008) Synthesis of C4-fluorinated solamins and their growth inhibitory activity against human cancer cell lines. *Bioorg. Med. Chem. Lett.* **18,** 6451–6453 CrossRef Medline
21. Potts, L. F., Luzzio, F. A., Smith, S. C., Hetman, M., Champy, P., and Litvan, I. (2012) Annonacin in *Asimina triloba* fruit: implication for neurotoxicity. *Neurotoxicology* **33,** 53–58 CrossRef Medline
22. Nishioka, H., Imoto, M., Imaoka, T., Sawa, T., Takeuchi, T., and Umezawa, K. (1994) Antitumor effect of piericidin B_1 *N*-oxide. *J. Antibiot.* (*Tokyo*) **47,** 447–452 CrossRef Medline
23. Kimura, K., Takahashi, H., Miyata, N., Yoshihama, M., and Uramoto, M. (1996) New piericidin antibiotics, 7-demethyl piericidin A_1 and 7-demethyl-3′-rhamnopiericidin A_1. *J. Antibiot.* (*Tokyo*) **49,** 697–699 CrossRef Medline
24. Escobar-Khondiker, M., Höllerhage, M., Muriel, M.-P., Champy, P., Bach, A., Depienne, C., Respondek, G., Yamada, E. S., Lannuzel, A., Yagi, T., Hirsch, E. C., Oertel, W. H., Jacob, R., Michel, P. P., Ruberg, M., *et al.* (2007) Annonacin, a natural mitochondrial complex I inhibitor, causes Tau pathology in cultured neurons. *J. Neurosci.* **27,** 7827–7837 CrossRef Medline
25. Masuya, T., Murai, M., Ifuku, K., Morisaka, H., and Miyoshi, H. (2014) Site-specific chemical labeling of mitochondrial respiratory complex I through ligand-directed tosylate chemistry. *Biochemistry* **53,** 2307–2317 CrossRef Medline
26. Masuya, T., Murai, M., Morisaka, H., and Miyoshi, H. (2014) Pinpoint chemical modification of Asp^{160} in the 49 kDa subunit of bovine mitochondrial complex I via a combination of ligand-directed tosyl chemistry and click chemistry. *Biochemistry* **53,** 7816–7823 CrossRef Medline
27. Murai, M., Sekiguchi, K., Nishioka, T., and Miyoshi, H. (2009) Characterization of the inhibitor binding site in mitochondrial NADH-ubiquinone oxidoreductase by photoaffinity labeling using a quinazoline-type inhibitor. *Biochemistry* **48,** 688–698 CrossRef Medline
28. Murai, M., Mashimo, Y., Hirst, J., and Miyoshi, H. (2011) Exploring interactions between the 49 kDa and ND1 subunits in mitochondrial NADH-ubiquinone oxidoreductase (complex I) by photoaffinity labeling. *Biochemistry* **50,** 6901–6908 CrossRef Medline
29. Banba, A., Tsuji, A., Kimura, H., Murai, M., and Miyoshi, H. (2019) Defining the mechanism of action of S1QELs, specific suppressors of superoxide production in the quinone-reaction site in mitochondrial complex I. *J. Biol. Chem.* **294,** 6550–6561 CrossRef Medline
30. Uno, S., Kimura, H., Murai, M., and Miyoshi, H. (2019) Exploring the quinone/inhibitor-binding pocket in mitochondrial respiratory complex I by chemical biology approaches, *J. Biol. Chem.* **294,** 679–696 CrossRef Medline
31. Tsukiji, S., Miyagawa, M., Takaoka, Y., Tamura, T., and Hamachi, I. (2009) Ligand-directed tosyl chemistry for protein labeling *in vivo*. *Nat. Chem. Biol.* **5,** 341–343 CrossRef Medline
32. Takaoka, Y., Ojida, A., and Hamachi, I. (2013) Protein organic chemistry and applications for labeling and engineering in live-cell systems. *Angew. Chem. Int. Ed. Engl.* **52,** 4088–4106 CrossRef Medline
33. Fiedorczuk, K., Letts, J. A., Degliesposti, G., Kaszuba, K., Skehel, M., and Sazanov, L. A. (2016) Atomic structure of the entire mammalian mitochondrial complex I. *Nature* **538,** 406–410 CrossRef Medline
34. Agip, A. A., Blaza, J. N., Bridges, H. R., Viscomi, C., Rawson, S., Muench, S. P., and Hirst, J. (2018) Cryo-EM structures of complex I from mouse heart mitochondria in two biochemically defined states. *Nat. Struct. Mol. Biol.* **25,** 548–556 CrossRef Medline
35. Brand, M. D., Goncalves, R. L. S., Orr, A. L., Vargas, L., Gerencser, A. A., Borch Jensen, M., Wang, Y. T., Melov, S., Turk, C. N., Matzen, J. T., Dardov, V. J., Petrassi, H. M., Meeusen, S. L., Perevoshchikova, I. V., Jasper, H., *et al.* (2016) Suppressors of superoxide-H_2O_2 production at site I_Q

of mitochondrial complex I protect against stem cell hyperplasia and ischemia-reperfusion injury. *Cell Metab.* **24,** 582–592 CrossRef Medline
36. Shiraishi, Y., Murai, M., Sakiyama, N., Ifuku, K., and Miyoshi, H. (2012) Fenpyroximate binds to the interface between PSST and 49 kDa subunits in mitochondrial NADH-ubiquinone oxidoreductase. *Biochemistry* **51,** 1953–1963 CrossRef Medline
37. Nakanishi, S., Abe, M., Yamamoto, S., Murai, M., and Miyoshi, H. (2011) Bis-THF motif of acetogenin binds to the third matrix-side loop of ND1 subunit in mitochondrial NADH-ubiquinone oxidoreductase. *Biochim. Biophys. Acta* **1807,** 1170–1176 CrossRef Medline
38. Rais, I., Karas, M., and Schägger, H. (2004) Two-dimensional electrophoresis for the isolation of integral membrane proteins and mass spectrometric identification, *Proteomics* **4,** 2567–2571 CrossRef Medline
39. Wong, H. S., Monternier, P. A., and Brand, M. D. (2019) S1QELs suppress mitochondrial superoxide/hydrogen peroxide production from site I_Q without inhibiting reverse electron flow through complex I. *Free Radic. Biol. Med.* **143,** 545–559 CrossRef Medline
40. Zickermann, V., Wirth, C., Nasiri, H., Siegmund, K., Schwalbe, H., Hunte, C., and Brandt, U. (2015) Mechanistic insight from the crystal structure of mitochondrial complex I. *Science* **347,** 44–49 CrossRef Medline
41. Blaza, J. N., Vinothkumar, K. R., and Hirst, J. (2018) Structure of the deactive state of mammalian respiratory complex I. *Structure* **26,** 312–319.e3 CrossRef Medline
42. Parey, K., Brandt, U., Xie, H., Mills, D. J., Siegmund, K., Vonck, J., Kühlbrandt, W., and Zickermann, V. (2018) Cryo-EM structure of respiratory complex I at work. *eLife* **7,** e39213 CrossRef Medline
43. Omura, S., Miyadera, H., Ui, H., Shiomi, K., Yamaguchi, Y., Masuma, R., Nagamitsu, T., Takano, D., Sunazuka, T., Harder, A., Kölbl, H., Namikoshi, M., Miyoshi, H., Sakamoto, K., and Kita, K. (2001) Anthelmintic compound, nafuredin, shows selective inhibition of complex I in helminth mitochondria. *Proc. Natl. Acad. Sci. U.S.A.* **98,** 60–62 CrossRef Medline
44. Shiomi, K., Ui, H., Suzuki, H., Hatano, H., Nagamitsu, T., Takano, D., Miyadera, H., Yamashita, T., Kita, K., Miyoshi, H., Harder, A., Tomoda, H., and Omura, S. (2005) A γ-lactone form nafuredin, nafuredin-γ, also inhibits helminth complex I. *J. Antibiot.* **58,** 50–55 CrossRef Medline
45. Murai, M., and Miyoshi, H. (2016) Current topics on inhibitors of respiratory complex I. *Biochim. Biophys. Acta* **1857,** 884–891 CrossRef Medline
46. Jeschke, P. (2016) Progress of modern agricultural chemistry and future prospects. *Pest Manag. Sci.* **72,** 433–455 CrossRef Medline
47. Fedor, J. G., Jones, A. J. Y., Di Luca, A., Kaila, V. R. I., and Hirst, J. (2017) Correlating kinetic and structural data on ubiquinone binding and reduction by respiratory complex I. *Proc. Natl. Acad. Sci. U.S.A.* **114,** 12737–12742 CrossRef Medline
48. Baradaran, R., Berrisford, J. M., Minhas, G. S., and Sazanov, L. A. (2013) Crystal structure of the entire respiratory complex I. *Nature* **494,** 443–448 CrossRef Medline
49. Uno, S., Masuya, T., Shinzawa-Itoh, K., Lasham, J., Haapanen, O., Shiba, T., Inaoka, D. K., Sharma, V., Murai, M., and Miyoshi, H. (2020) Oversized ubiquinones as molecular probes for structural dynamics of the ubiquinone reaction site in mitochondrial respiratory complex I. *J. Biol. Chem.* **295,** 2449–2463 CrossRef Medline
50. Parey, K., Haapanen, O., Sharma, V., Köfeler, H., Züllig, T., Prinz, S., Siegmund, K., Wittig, I., Mills, D. J., Vonck, J., Kühlbrandt, W., and Zickermann, V. (2019) High-resolution cryo-EM structures of respiratory complex I: mechanism, assembly, and disease. *Sci. Adv.* **5,** eaax9484 CrossRef Medline
51. Treberg, J. R., Quinlan, C. L., and Brand, M. D. (2011) Evidence for two sites of superoxide production by mitochondrial NADH-ubiquinone oxidoreductase (complex I). *J. Biol. Chem.* **286,** 27103–27110 CrossRef Medline
52. Orr, A. L., Ashok, D., Sarantos, M. R., Shi, T., Hughes, R. E., and Brand, M. D. (2013) Inhibitors of ROS production by the ubiquinone-binding site of mitochondrial complex I identified by chemical screening. *Free Radic. Biol. Med.* **65,** 1047–1059 CrossRef Medline
53. Fernández-Agüera, M. C., Gao, L., González-Rodríguez, P., Pintado, C. O., Arias-Mayenco, I., García-Flores, P., García-Pergañeda, A., Pascual, A., Ortega-Sáenz, P., and López-Barneo, J. (2015) Oxygen sensing by arterial chemoreceptors depends on mitochondrial complex I signaling. *Cell Metab.* **22,** 825–837 CrossRef Medline
54. Mills, E. L., Kelly, B., Logan, A., Costa, A. S. H., Varma, M., Bryant, C. E., Tourlomousis, P., Däbritz, J. H. M., Gottlieb, E., Latorre, I., Corr, S. C., McManus, G., Ryan, D., Jacobs, H. T., Szibor, M., *et al.* (2016) Succinate dehydrogenase supports metabolic repurposing of mitochondria to drive inflammatory macrophages. *Cell* **167,** 457–470.e13 CrossRef Medline
55. Baccelli, I., Gareau, Y., Lehnertz, B., Gingras, S., Spinella, J.-F., Corneau, S., Mayotte, N., Girard, S., Frechette, M., Blouin-Chagnon, V., Leveillé, K., Boivin, I., MacRae, T., Krosl, J., Thiollier, C., *et al.* (2019) Mubritinib targets the electron transport chain complex I and reveals the landscape of OXPHOS dependency in acute myeloid leukemia. *Cancer Cell* **36,** 84–99.e8 CrossRef Medline
56. Madhusudhan, N., Hu, B., Mishra, P., Calva-Moreno, J. F., Patel, K., Boriack, R., Ready, J. M., and Nijhawan, D. (2020) Target discovery of selective non-small-cell lung cancer toxins reveals inhibitors of mitochondrial complex I. *ACS Chem. Biol.* **15,** 158–170 CrossRef Medline
57. Matsuno-Yagi, A., and Hatefi, Y. (1985) Studies on the mechanism of oxidative phosphorylation. *J. Biol. Chem.* **260,** 11424–11427 Medline
58. Ernster, L., and Lee, C.-P. (1967) Energy-linked reduction of NAD^+ by succinate. *Methods Enzymol.* **10,** 729–738 CrossRef
59. Laemmli, U. K. (1970) Cleavage of structural proteins during the assembly of the head of bacteriophage T4. *Nature* **227,** 680–685 CrossRef Medline
60. Schägger, H. (2006) Tricine-SDS-PAGE. *Nat. Protoc.* **1,** 16–22 CrossRef Medline
61. Pravda, L., Sehnal, D., Toušek, D., Navrátilová, V., Bazgier, V., Berka, K., Svobodová Vařeková, R., Koča, J., and Otyepka, M. (2018) MOLEonline: a web-based tool for analyzing channels, tunnels and pores. *Nucleic Acids Res.* **46,** W368–W373 CrossRef Medline